Centrum voor Wiskunde en Informatica

Centre for Mathematics and Computer Science

P.W. Hemker

Defect correction and higher order schemes for the multigrid solution of the steady Euler equations

Department of Numerical Mathematics Report NM-R8523 November

1985

Centrum voor Wiskunde en Informatica
Centre for Mathematics and Computer Science

P.W. Hemker

Defect correction and higher order schemes for the multigrid solution of the steady Euler equations

Department of Numerical Mathematics Report NM-R8523 November

The Centre for Mathematics and Computer Science is a research institute of the Stichting Mathematisch Centrum, which was founded on February 11, 1946, as a nonprofit institution aiming at the promotion of mathematics, computer science, and their applications. It is sponsored by the Dutch Government through the Netherlands Organization for the Advancement of Pure Research (Z.W.O.).

Defect Correction and Higher Order Schemes for the Multigrid Solution of the Steady Euler Equations

P.W. Hemker
Centre for Mathematics and Computer Science
P.O. Box 4079, 1009 AB Amsterdam, The Netherlands

In this paper we describe 1st and 2nd order finite volume schemes for the solution of the steady Euler equations for inviscid flow. The solution for the first order scheme can be efficiently computed by a FAS multigrid procedure. Second order accurate approximations are obtained by linear interpolation in the flux- or the state space. The corresponding discrete system is solved (up to truncation error) by defect correction iteration. An initial estimate for the 2nd order solution is computed by Richardson extrapolation. Examples of computed approximations are given, with emphasis on the effect for the different possible discontinuities in the solution.

1980 Mathematics Subject Classification: 65N05, 65N30, 76G13.
Key Words & Phrases: steady Euler equations, multigrid methods, higher order schemes, defect correction
Note: This report will be submitted for publication elsewhere.

1. INTRODUCTION

As soon as viscosity and heat conduction are neglected, the flow of a gas is described by the Euler equations. In two dimensions these equations are given by

$$\frac{\partial q}{\partial t} + \frac{\partial}{\partial x} f(q) + \frac{\partial}{\partial y} g(q) = 0 , \tag{1.1}$$

with

$$q = \begin{bmatrix} \rho \\ \rho u \\ \rho v \\ \rho e \end{bmatrix} , \quad f = \begin{bmatrix} \rho u \\ \rho u^2 + p \\ \rho uv \\ \rho uH \end{bmatrix} , \quad g = \begin{bmatrix} \rho v \\ \rho vu \\ \rho v^2 + p \\ \rho vH \end{bmatrix} , \tag{1.2}$$

where ρ , u , v , e and p respectively represent density, velocity in x- and y- direction, specific energy and pressure; $H = e + p / \rho$ is the specific enthalpy. The pressure is obtained from the equation of state, which - for a perfect gas - reads

$$p = (\gamma - 1)\rho(e - \tfrac{1}{2}(u^2 + v^2)),$$

γ is the ratio of specific heats. $q(t,x,y)$ describes the state of the gas as a function of time and space and f and g are the flux in the x- and y- direction. We denote the open domain of definition of (1.1)

by Ω^* .

It is well known that solutions of the nonlinear equations (1.1) may develop discontinuities, even if the initial flow ($t=t_0$) is smooth. To allow discontinuous solutions, (1.1) is rewritten in its integral form

$$\frac{\partial}{\partial t}\iint_{\Omega} q\, dx\, dy \;+\; \int_{\partial\Omega}(f.n_x + g.n_y)\, ds \;=\; 0\,, \qquad \text{for all } \Omega\subset\Omega^*\,; \tag{1.3}$$

$\partial\Omega$ is the boundary of Ω and (n_x,n_y) is the outward normal vector at the boundary $\partial\Omega$.

The form (1.3) of equation (1.1) shows clearly the character of the system of conservation laws: the increase of q in Ω can be caused only by the inflow of q over $\partial\Omega$. In symbolic form we write (1.1) as

$$q_t + N(q) = 0. \tag{1.4}$$

In the numerical computations we are only interested in the solution of the steady state Euler equations

$$N(q) = 0. \tag{1.5}$$

The solution of the weak form (1.3) of (1.1) is known to be non-unique and a physically realistic solution (which is the limit of a flow with vanishing viscosity) is known to satisfy the additional entropy condition (cf. [15,16]). Further, the equation (1.1) is hyperbolic, i.e. written in the form

$$\frac{\partial q}{\partial t} + \frac{\partial f}{\partial q}.\frac{\partial q}{\partial x} + \frac{\partial g}{\partial q}.\frac{\partial q}{\partial y} = 0$$

the matrix

$$k_1\frac{\partial f}{\partial q} + k_2\frac{\partial g}{\partial q}$$

has real eigenvalues for all (k_1,k_2).

These eigenvalues are $(k_1u+k_2v)\pm c$ and (k_1u+k_2v) (a double eigenvalue); $c = \sqrt{\gamma p/\rho}$ is the local speed of sound. The sign of the eigenvalues determines the direction in which the information about the solution is carried along the line (k_1,k_2) as time develops (the direction of the characteristics). It locates the domain of dependence. The entropy condition implies that characteristics do not emerge at a discontinuity in the flow.

2. THE BASIC DISCRETIZATION

In order to discretize eq. (1.1) on a domain with an irregular grid, there are two ways to proceed. First, a mapping can be defined from the physical domain to a computational domain, so that the irregular grid in the physical domain corresponds to a regular grid in the computational domain. By means of this transformation the equation and the boundary conditions are reformulated for the computational domain, where they will contain metric information about the mapping. Now an (arbitrarily accurate) discretization of the transformed equations can be used on the regular grid to solve the original problem.

A second approach (a *finite volume* technique) is to divide the domain of definition in the physical space into a number of disjunct cells $\{\Omega_\alpha\}$ and to require the equation (1.3) to hold on each $\bigcup\Omega_\alpha$. In this way the essential global property of the flow -the conservation character- is easily preserved as long as we take care that for any two neighboring cells Ω_α and Ω_β with $\Gamma_{\alpha\beta} = \partial\bar{\Omega}_\alpha \bigcup \partial\bar{\Omega}_\beta$, the same approximation is used for the flow quantities $\int_{\Gamma_{\alpha\beta}} f.n_x + g.n_y\, ds$, both for the outflow of Ω_α and for the inflow of Ω_β . In that case (1.3) will hold for any Ω which is the union of an arbitrary subset of $\{\Omega_\alpha\}$. In this approach there is no need to transform the equations (1.1) or the boundary conditions.

We found it most convenient to use this finite volume technique and to divide the domain Ω^* in

quadrilateral cells Ω_{ij} in a way that is topologically equivalent with a regular division in squares (i.e. $\Omega_{i\pm1,j\pm1}$ are the only possible neighbors of Ω_{ij}).

In order to define subsequent refinements of the irregular mesh and to define a meaningful order of accuracy for our schemes on these non-uniform grids, we introduce a mapping from a "computational domain" divided into regular squares, to the physical domain Ω^*. We assume this mapping to be non-singular (i.e. with a non-vanishing Jacobian J on $\overline{\Omega}^*$) and sufficiently smooth (bounded partial derivatives of J).

The discrete approximation $\tilde{q}(t,x,y)$ to $q(t,x,y)$ is represented by the values q_{ij} for each Ω_{ij}, where q_{ij} represents the mean value of $\tilde{q}$ over Ω_{ij}

$$q_{ij} \approx \frac{\int\int_{\Omega_{ij}} \tilde{q}(x,y)\, dx\, dy}{\text{meas}(\Omega_{ij})}. \tag{2.1}$$

The space discretization method is now completely determined by the way of approximating

$$\int_{\Gamma_{ijk}} (f.n_x + g.n_y)\, ds\,, \qquad k = 1,2,3,4, \tag{2.2}$$

at the four walls of the quadrilateral cell Ω_{ij}. The wall Γ_{ijk} may be either a common boundary with another cell Ω_{ijk} or a part of the boundary $\partial\Omega^*$. In the first case we have to take into account the requirement of conservation of q. To satisfy this requirement we compute the approximation of (2.2) as

$$f^k(q_{ij}^k, q_{ijk}^k) \cdot \text{meas}(\Gamma_{ijk}), \tag{2.3}$$

i.e. we approximate $fn_x + gn_y$ by a constant value at Γ_{ijk}, which depends only on q_{ij}^k, a uniform (constant) approximation to $\tilde{q}(t,x,y)$ in Ω_{ij} at the wall Γ_{ijk}, and on q_{ijk}^k, a similar approximation to $\tilde{q}(t,x,y)$ in Ω_{ijk} at Γ_{ijk}. (Notice that $\tilde{q}(t,x,y)$ is not assumed to be continuous over Γ_{ijk} .)

The semi-discretization of the equations (1.4) is now

$$\frac{\partial}{\partial t} q_h \,|_{i,j} = -N_h(q_h)\,|_{i,j} := -\frac{\sum_{k=1,2,3,4} f^k(q_{ij}^k, q_{ijk}^k)\, \text{meas}(\Gamma_{ijk})}{\text{meas}(\Omega_{ij})}\,, \tag{2.4}$$

and the steady discrete equations $N_h(q_h) = 0$ are equivalent with

$$\sum_{k=1,2,3,4} f^k(q_{ij}^k, q_{ijk}^k) \cdot \text{meas}(\Gamma_{ijk}) = 0, \qquad \text{for all } \Omega_{ij} \subset \Omega^*\,. \tag{2.5}$$

The approximate flux function $f^k(q_{ij}^k, q_{ijk}^k)$ depends on the direction (n_x^k, n_y^k), of the side Γ_{ijk}. However, by the rotation invariance of the Euler equations, we may relate $f^k(\,.\,,\,.\,)$ to a local coordinate system (rotated such that it is aligned with Γ_{ijk}). Hence, only a single function $f(\,.\,,\,.\,)$, the *numerical flux function,* is needed to approximate the flux between two cells (cf.[9,10]):

$$f(\,.\,,\,.\,) = f^k(\,.\,,\,.\,) \quad \text{if} \quad n_x^k = 1,\ n_y^k = 0\,. \tag{2.6}$$

In this way the freedom in the approximation of (2.3) is in the choice of a numerical flux function and in the computation of q_{ij}^k and q_{ijk}^k from $\{q_{ij} | \Omega_{ij} \subset \Omega^*\}$. We shall first consider two elementary possibilities for the choice of a numerical flux function. Then we describe the computation of $\{q_{ij}^k\}$ for the first order scheme. In the next section we shall consider second order schemes, generated by other computations of $\{q_{ij}^k\}$ or f^k .

For consistency of the resulting scheme, $f(\,.\,,\,.\,)$ should satisfy $f(q,q) = f(q)$, cf. [7]. A usual representation of $f(\,.\,,\,.\,)$ is given by

$$f(q_0,q_1) = \tfrac{1}{2} f(q_0) + \tfrac{1}{2} f(q_1) - \tfrac{1}{2}\, d(q_0,q_1), \tag{2.7}$$

with $d(q_0,q_1) = \mathcal{O}(\,|\,|q_1 - q_0|\,|\,)$.

The *central difference flux* is defined by $d(q_0,q_1) = 0$. For an *upwind* numerical flux functions we have ([7]),

$$d(q_0,q_1) = \left| \frac{\partial f}{\partial q}\left[\frac{q_0 + q_1}{2}\right] \right| (q_1 - q_0) + o(||q_1 - q_0||). \tag{2.8}$$

For reasons explained in [10], we prefer to use a slight modification of a numerical flux function that was proposed by Osher [19,21]. We take

$$d(q_0,q_1) = \int_{q_0}^{q_1} |\frac{\partial f}{\partial q}|(w)\, dw\ , \tag{2.9}$$

where the integration path in the state space follows three sub-paths along the eigenspaces of $\partial f / \partial q$. These sub-paths correspond to the eigenvalues $\lambda_1 = u - c$, $\lambda_2 = \lambda_3 = u$, and $\lambda_4 = u + c$ respectively.

In the case that $\Gamma_{ijk} \subset \partial\Omega^*$, interpolation from the interior of Ω^* yields a value q_{ijk}^{IN} which corresponds to the mean value of $\tilde{q}_{ij}$ at Γ_{ijk} in Ω_{ij}:

$$q_{ijk}^{IN} = \frac{\int_{\Gamma_{ijk}} \tilde{q}(t,x,y)\ ds}{\text{meas}(\Gamma_{ijk})}\ .$$

For well posed boundary conditions $B(q) = 0$ at Γ_{ijk} , a value q_{ijk}^{OUT} can be determined such that

$$f^k(q_{ijk}^{OUT}, q_{ijk}^{IN}) = f^k(q_{ijk}^{OUT}), \tag{2.10a}$$

and

$$B(q_{ijk}^{OUT}) = 0 \tag{2.10b}$$

is satisfied at a point on Γ_{ijk} . In [10] we showed how q_{ijk}^{OUT} is connected with q_{ijk}^{IN} with respect to the outgoing characteristics; the incoming characteristic information is taken from the boundary conditions. This corresponds with the use of Riemann invariants to derive non-reflecting numerical boundary conditions.

In our first order scheme we use a piecewise constant numerical approximation for $\tilde{q}$:

$$q(x,y) = q_{ij} \qquad \text{for} \quad (x,y) \in \Omega_{ij}. \tag{2.11a}$$

This uniform state in Ω_{ij} is assumed for all (i,j), and hence

$$f^k(q_{ij}^k, q_{ijk}^k) = f^k(q_{ij}, q_{ijk})\ . \tag{2.11b}$$

The flux at Γ_{ijk} now corresponds with the flux at a discontinuity between two uniform states. Such a flux can be computed by solving the Riemann problem of gasdynamics. However, this is a nontrivial nonlinear computation, and we approximate it by (2.7) , (2.9), cf.[10], which is a slight variant of Osher's "approximate Riemann solver".

The order of accuracy of the resulting schemes on the nonuniform mesh is not immediate. It can be proved that in general (at most) second order accuracy can be obtained when q_{ij}^k, q_{ijk}^k are computed properly. We shall give here the principles along which these accuracy results are derived. For the detailed proof see [23].

The relation between equation (1.1) and (2.4) can be described by the following diagram

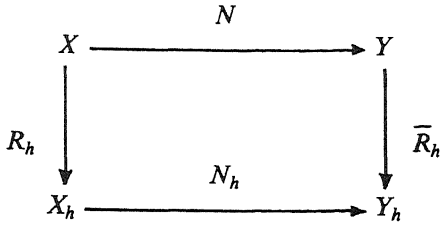

where X (X_h) and Y (Y_h) are the continuous (discrete) spaces of state and change-of-state respectively: $q \in X$, $q_h \in X_h$, $N(q) \in Y$, $N_h(q_h) \in Y_h$.

To compute the order of consistency, we introduce the restrictions R_h and $\bar{R}_h$, as well as the parametrization $h \to 0$ for the mesh refinement.

For a given parameter value $h > 0$, and an arbitrary $q \in X$ we define

$$\bar{q}(\xi,\eta) = \frac{1}{(2h)^2} \cdot \int_{\xi-h}^{\xi+h} \int_{\eta-h}^{\eta+h} q(x(\xi,\eta),y(\xi,\eta)) \; d\xi \; d\eta \cdot \tag{2.12}$$

Here $x(\xi,\eta)$ and $y(\xi,\eta)$ describe the mapping between the computational (ξ,η)-domain and the physical (x,y)-domain, such that

$$(x(2hi \pm h, 2hj \pm h) \, , \, y(2hi \pm h, 2hj \pm h)) \tag{2.13}$$

denote the vertices of the cell Ω_{ij} in the physical space. We consider the order of consistency for the discretization on the irregular grid, assuming that the mesh refines corresponding to $h \to 0$ in (2.13), and that the mapping $(\xi,\eta) \to (x,y)$ is independent of h. Moreover, we require the Jacobian $J(\xi,\eta) = x_\xi y_\eta - x_\eta y_\xi$ not to vanish and to be smooth enough, i.e. $|J(\xi,\eta)| \geq C_1 > 0$, and

$$\left| \left[\frac{\partial}{\partial \xi}\right]^{m_1} \left[\frac{\partial}{\partial \eta}\right]^{m_2} J(\xi,\eta) \right| \leq C_2 \, |J(\xi,\eta)| \, .$$

A mean value of q in Ω_{ij} is now given by $\bar{q}(2hi, 2hj)$. In this way a restriction operator R_h: $q \to q_h$ is defined.

Notice that the assumptions on the Jacobian imply

$$\frac{\iint_{\Omega_{ij}} q \; dx \; dy}{\iint_{\Omega_{ij}} dx \; dy} = \bar{q}(2hi, 2hj) \, (1 + \mathcal{O}(h^2)) \cdot \tag{2.14}$$

The restriction $\bar{R}_h$: $Y \to Y_h$ is simply defined by

$$(\bar{R}_h r)_{i,j} = \frac{1}{(2h)^2} \cdot \iint_{\Omega_{ij}} r \; dx \, dy \, . \tag{2.15}$$

Now the truncation error for $q \in X$ is defined as

$$N_h (R_h q) - \bar{R}_h N(q) = \tau_h(q), \tag{2.16}$$

and for a smooth function q we can determine the order of consistency. It can be shown that the order of consistency is 1 if eq.(2.11) holds. We denote this first order semi-discretization (2.4) - (2.11) in symbolic form by

$$(q_h)_t + N_h^1(q_h) = 0 \, . \tag{2.17}$$

Note: In the actual computations each discrete equation at the h-level is multiplied by a factor $(2h)^2$. This can be seen as discretization of the integral form (1.3) rather than of the differential form (1.1). The advantage is a simpler implementation.

3. SECOND ORDER SCHEMES

The first order discretization discussed in section 2 has a number of advantages: it is conservative, satisfies an entropy condition, is monotonous and gives a sharp representation of discontinuities (shocks and contact discontinuities), as long as these are aligned with the mesh. Further it allows an efficient solution of the discrete equations by a multigrid method [9]. Disadvantages are: the low order of accuracy (many points are required to find an accurate representation of a smooth solution) and the fact that it is highly diffusive for oblique discontinuities (the discontinuities are smeared out over a large number of cells). For a first order (upwind) scheme these are well known facts (cf. e.g. [8]) and it leads to the search for higher order methods.

A key property of the discretization, that we want to maintain in a 2nd order scheme, is the conservation of q, because it allows discontinuities to be captured as weak solutions of (1.1) and avoids the necessity of a shock fitting technique. Therefore, we consider only schemes that are still based on (2.4), and we select $f^k(q_{ij}^k, q_{ijk}^k)$ that yield a better approximation to (2.2) than (2.11b).

The higher order schemes can be obtained in two different ways. Higher order interpolation (or extrapolation) is used either for the states (i.e. in X_h) or for the fluxes (i.e. in Y_h). The first approach is used e.g. in [1,4,28], the second in [20,24]. In the first case, in (2.5) q_{ij}^k and q_{ijk}^k are obtained by some interpolation from $q_h = \{q_{ij}\}$. In the latter, $f^k(q_{ij}^k, q_{ijk}^k)$ is obtained from $\{f^k(q_{ij}^k, q_{ijk}^k)\} \bigcup \{f^k(q_{ij}^k, q_{ij}^k)\}$

From the point of view of finite volume discretization, a straightforward way to form a more accurate approximation is to replace the 1st order approximation (2.11) by a 2nd order one. Instead of the piecewise constant $\tilde{q}(x,y)$, we may consider a piecewise bilinear function $\tilde{q}(x,y)$ on a set of 2×2 cells (a "superbox"). Such a superbox on the h-level corresponds with a single cell at the 2h-level. Over the boundaries of the superbox $\tilde{q}(x,y)$ can be discontinuous; in the superbox $\tilde{q}(x,y)$ is determined by q_{ij}, $q_{i+1,j}$, $q_{i,j+1}$ and $q_{i+1,j+1}$ as defined by (2.1). Using such a bilinear function, we see that the central difference approximation is used for flux computations inside the superboxes; at superbox boundaries interpolation is made from the left and the right and the approximate Riemann solver is used to compute the flux. We denote the corresponding discrete operator by N_h^S. It is easily shown that this *superbox scheme* is 2nd order accurate in the sense that

$$\overline{R}_{2h,h}\,(N_h^S(R_h q) - \overline{R}_h N(q)) = \mathcal{O}(h^2)\,.$$

Instead of the finite volume superbox scheme, we can also adopt a finite difference approach. In the case of interpolation of states, interpolation from the left (right) can be used to obtain a value q_{ijk}^L (q_{ijk}^R) at the left (right) side of all walls Γ_{ijk}. In the case of interpolation of fluxes, it may be necessary to split flux-differences in positive and negative (right- and left- going) parts.

In both cases the simplest 2nd order schemes are central differencing schemes. Here the interpolation is done irrespective of a particular characteristic direction. Central differencing in the X_h-space yields $f(q_0,q_1) = f((q_0 + q_1)/2)$ for the numerical flux function (2.6). By central differencing in Y_h we obtain $f(q_0,q_1) = \frac{1}{2}f(q_0) + \frac{1}{2}f(q_1)$. In contrast with the first order schemes, the central difference schemes are under-diffusive, which may lead to instabilities. An uncoupling of odd and even points may occur and spurious oscillations may appear in the solution. When these schemes are used alone, an artificial additional diffusion (dissipation) term is added to stabilize the solution [11,22].

To improve the stability behavior, both for the X_h- and for the Y_h-interpolation, it is better to take into account the domain of dependence of the solution (the direction of the characteristics) and to distinguish between interpolation from the left and from the right of a cell wall. For simplicity of notation we shall exemplify this only for the 1-D case. Generalization to 2-D is straightforward.
In 1-D , eq.(2.4) reduces to

$$N_h(q_h)_i = \frac{f_{i+\frac{1}{2}} - f_{i-\frac{1}{2}}}{x_{i+\frac{1}{2}} - x_{i-\frac{1}{2}}}\,, \tag{3.1}$$

where $f_{i+\frac{1}{2}} = f(q^L_{i+\frac{1}{2}}, q^R_{i+\frac{1}{2}})$.

Interpolation in X_h

At a cell wall $x_{i+1/2}$ we distinguish between the interpolated values from the left, $q^L_{i+1/2}$, and from the right, $q^R_{i+1/2}$. We define $\Delta q_{i+1/2} = q_{i+1} - q_i$ and find the 2nd order upwind interpolated values

$$q^L_{i+\frac{1}{2}} = q_i + \frac{1}{2}\,\Delta q_{i-\frac{1}{2}}\,, \tag{3.2}$$
$$q^R_{i+\frac{1}{2}} = q_{i+1} - \frac{1}{2}\,\Delta q_{i+\frac{3}{2}}\,.$$

The stability properties of these one-sided approximations are better than for central approximations, but monotonicity is not preserved (see section 5). The usual way to force the monotonicity is to introduce a limiting function ϕ, $0 \leqslant \phi \leqslant 2$ and to interpolate by

$$q^L_{i+\frac{1}{2}} = q_i + \frac{1}{2}\,\phi^L_{i+\frac{1}{2}}\,\Delta q_{i-\frac{1}{2}} \tag{3.3}$$
$$q^R_{i-\frac{1}{2}} = q_i - \frac{1}{2}\,\phi^R_{i-\frac{1}{2}}\,\Delta q_{i+\frac{1}{2}}\,,$$

where ϕ^L and ϕ^R are chosen depending on $\{\Delta q_{i\pm\frac{1}{2}}\}$ such that $q^L_{i-1/2}$ lies between q_{i-1} and q_i, and $q^R_{i+1/2}$ between q_i and q_{i+1}, (cf. [1,26]).

Van Leer [28] also introduces a linear combination of the one-sided and central interpolation. Parametrized by κ we obtain

$$q^L_{i+\frac{1}{2}} = q_i + \frac{1}{4}\left[(1-\kappa)\Delta q_{i-\frac{1}{2}} + (1+\kappa)\Delta q_{i+\frac{1}{2}}\right], \tag{3.4}$$
$$q^R_{i-\frac{1}{2}} = q_i - \frac{1}{4}\left[(1-\kappa)\Delta q_{i+\frac{1}{2}} + (1+\kappa)\Delta q_{i-\frac{1}{2}}\right].$$

This formula contains: ($\kappa = -1$) the one-sided 2nd order scheme, ($\kappa = \frac{1}{3}$) a "3rd order" upwind biased scheme, and ($\kappa = 1$) the central difference scheme. (Notice that the "3rd order" scheme is 3rd order consistent in a 1-D situation; in 2-D the scheme is still 2nd order accurate.) We use (2.4) - (3.4) for the construction of a 2nd order discretization of (1.4)

$$(q_h)_t + N^2_h(q_h) = 0\,. \tag{3.5}$$

In 1-D the superbox scheme corresponds to the use of $\kappa = +1$ for odd i, and $\kappa = -1$ for even i.

The interpolation (3.4) is well defined in the interior cells of the domain. In the cells near the boundary $\partial\Omega^*$, one of the values $\Delta q_{i\pm1/2}$ is not defined, by the absence of a value q_i corresponding to a point outside Ω^*. Here a different approximation should be used. In our computations we set $\Delta q_{i+1/2} = \Delta q_{i-1/2}$ at the cell Ω_i near the boundary. This corresponds with the "superbox" approximation for these cells. For the superbox scheme and for the scheme (3.4), with different values of κ, we show some results in section 5.

Interpolation in Y_h

To take into account the domain of dependence (the direction of the characteristics), we here distinguish between flux differences in the positive and in the negative direction. We define

$$\Delta f^+_{i+\frac{1}{2}} = -f(q_i, q_{i+1}) + f(q_{i+1}), \tag{3.6}$$
$$\Delta f^-_{i+\frac{1}{2}} = +f(q_i, q_{i+1}) - f(q_i).$$

It is easily seen that

$$f(q_{i+1}) - f(q_i) = \Delta f^+_{i+\frac{1}{2}} + \Delta f^-_{i+\frac{1}{2}}\,,$$

and

$$f(q_i,q_{i+1}) - f(q_{i-1},q_i) = \Delta f^+_{i-\frac{1}{2}} + \Delta f^-_{i+\frac{1}{2}} .$$

Further, the numerical flux has been constructed such that

$$\Delta f^+_{i+\frac{1}{2}} \;/\; \Delta q_{i+\frac{1}{2}} \geqslant 0 , \tag{3.7}$$

$$\Delta f^-_{i+\frac{1}{2}} \;/\; \Delta q_{i+\frac{1}{2}} \leqslant 0.$$

For vectors f and q we mean by (3.7) that the matrices of partial derivatives have real non-negative (non-positive) eigenvalues. Hence, $\Delta f^+_{i+\frac{1}{2}}$ (or $\Delta f^-_{i+\frac{1}{2}}$) corresponds to information going to the right (left).

A 2nd order upwind scheme is now constructed as

$$f^k_{i+\frac{1}{2}} := f^k(q_i,q_{i+1}) + \tfrac{1}{2}\,\Delta f^+_{i-\frac{1}{2}} - \tfrac{1}{2}\Delta f^-_{i+\frac{3}{2}} \tag{3.8}$$

Notice that with this notation central differencing is written as

$$f^k_{i+\frac{1}{2}} := f^k(q_i,q_{i+1}) + \tfrac{1}{2}\,\Delta f^+_{i+\frac{1}{2}} - \tfrac{1}{2}\Delta f^-_{i+\frac{1}{2}} . \tag{3.9}$$

Also here a linear combination of (3.8) and (3.9) is easily realized and flux limiting functions can be introduced to maintain monotonicity of the solution as for (3.3) [20].

4. DEFECT CORRECTION ITERATION

The 2nd order space discretization of the timedependent equations (1.4) yields a semi-discretization (3.5). The usual way to find the solution of the steady state equations

$$N^2_h(q_h) = 0 , \tag{4.1}$$

is to take an initial guess and to solve (3.5) for $t\to\infty$, i.e. to compute $q_h(t)$ until initial disturbances have sufficiently died out. The advantage is that, starting with a physically meaningful situation, we may expect that a meaningful steady state will be reached, even when unicity of the steady equations is not guaranteed. The drawback is that many timesteps may be necessary before the solution has sufficiently converged. For the acceleration of the convergence, many devices have been developed such as local time stepping, residual smoothing, implicit residual averaging or enthalpy damping [22].

Multigrid is also used as an acceleration device [14,18,22]. Here discretizations (3.5) are given on a sequence of grids. The coarse grids are used to move low frequency disturbances rapidly out of the domain Ω^* by large timesteps, whereas high frequency disturbances should be locally damped on the fine grids, e.g. by a sufficiently dissipative timestepping procedure.

We take another approach [9,10,12,13,17], and consider directly the steady state equations. By the stability of the first order discretization, a relatively simple relaxation method (Collective Symmetric Gauss Seidel iteration, i.e. a SGS relaxation where the 4 variables corresponding to a single cell Ω_{ij} are relaxed collectively) is able to reduce the high frequency error components efficiently, and -therefore- a FAS-algorithm with this relaxation is well suited to solve the discrete first order equations.

Although no explicit artificial viscosity is added to the scheme, a suitable amount of "numerical diffusivity" is automatically introduced by the upwind discretization. As $h\to 0$, this "artificial diffusion" vanishes and the sequence of discretizations converges to the Euler equations as the limit of an equation with vanishing viscosity.

Another advantage of the introduction of this "artificial viscosity" just by the use of the upwind scheme is that the coarser discretizations, including their larger amount of "numerical viscosity", are now Galerkin approximations to the corresponding finer grid discretizations. Hence coarse and fine discretizations are relatively consistent. (For a discussion of related problems when multigrid is

applied to the convection diffusion equation and various amounts of artificial viscosity are used on the different grids cf [30].)

When we try to solve the 2nd order discretization (4.1) in the same manner as we do the first order equations, we may expect difficulties for two reasons. First, the set of 4 equations to be solved at each cell Ω_{ij} in the Collective SGS relaxation is much more complex . The set up of these equations would increase the amount of computational work considerably. Secondly, the nonlinear equations (4.1) are less stable. The 2nd order discretizations are less diffusive, and in the case of central differences clearly "anti-diffusive". This may lead not only to non-monotonous solutions, but it also can cause a Gauss Seidel relaxation not to reduce sufficiently the rapidly varying error components.

A local mode analysis of smoothing properties of GS for 1st and 2nd order upwind Euler discretizations can be found in [12]. There, the flux splitting upwind scheme of Steger and Warming[25] is analyzed, whereas we apply Osher's scheme [19,21]. Numerical evidence that convergence for the relaxation process of a 2nd order upwind procedure is slower than for a 1st order scheme, is also found in [17,29]. Here van Leer's flux splitting scheme [27] was used.

To obtain 2nd order accurate solutions, we do not try to solve the system $N_h^2(q_h) = 0$ as such. We use the first order operator N_h^1 to find the higher order accurate approximation in a defect correction iteration:

$$N_h^1(q_h^{(1)}) = 0\,, \tag{4.2a}$$

$$N_h^1(q_h^{(i+1)}) = N_h^1(q_h^{(i)}) - N_h^2(q_h^{(i)}). \tag{4.2b}$$

For an introduction to the defect correction principle see [2]. It is well known [6] that -if the problem is smooth enough- the accuracy of $q_h^{(i)}$ is of order 2 for $i \geqslant 2$. If the solution is not smooth (higher order derivatives are dominating) there is no clear reason to expect the solution of (4.1) to be more accurate than the solution of (4.2a). Nevertheless, in section 5 evidence is given that a few defect correction steps may improve the solution considerably.

In fact we may use $q_h^{(i+1)} - q_h^{(i)}$ as an error indicator. In the smooth parts of the solution $q_h^{(1)} - q_h^{(1+i)} = \mathcal{O}(h)$, $q_h^{(2)} - q_h^{(2+i)} = \mathcal{O}(h^2)$; where these differences are larger, e.g. $\mathcal{O}(1)$, the solution is not smooth (relative to the the grid used). Then grid adaptation is to be considered rather than the choice of a higher order method, if a more accurate solution is wanted.

In a multigrid environment, where solutions on more grids are available, we should -of course- also consider other approaches to compute higher order solutions, such as

(1) Richardson extrapolation,

(2) τ-extrapolation, or

(3) Brandt's double discretization.

The two extrapolation methods can be well used to find a more accurate solution if the solution is smooth indeed. Then no additional difference scheme (4.1) is required . A drawback is that these methods rely on the existence of an asymptotic expansion of the (truncation) error for $h \rightarrow 0$, and -globally- no a-priori information about the validity of this assumption is available. Another disadvantage is that the accurate solution (for Richardson extrapolation) or the estimate for the truncation error (τ-extrapolation) is obtained at the one-but-finest level and no high resolution of local phenomena is obtained. Whereas we want not only a high order of accuracy, but also an accurate representation of possible discontinuities, we use Richardson extrapolation (only) as a possibility to find a higher order initial estimate for the iteration process (4.2b).

Since the evaluation of $N_h^2(q_h)$ is hardly more expensive than the evaluation of $N_h^1(q_h)$, the costs to compute the defect in (4.2b) is of the same order as the evaluation of the relative truncation error $\tau_{2h,h}(q_h) = N_{2h}^1(R_{2h,h}q_h) - R_{2h,h}N_h^1(q_h)$. This makes us to prefer (4.2b) to τ-extrapolation.

Having both a 1st and a 2nd order discrete operator at our disposal, Brandt's double discretization [3] seems another efficient way to find a 2nd order accurate solution. However, we have bad experience in applying it to the Euler equations. In particular when solving (contact) discontinuities. Using the Collective SGS relaxation and a 2nd order scheme based on (3.4), we experienced serious problems in the computation of the numerical fluxes (2.11b), caused by virtual cavitation of the flow. Our

explanation is the following. In Brandt's double discretization each iteration cycle consists of a smoothing step towards the solution of $N_h^1(q_h) = r_h^1$, and a coarse grid correction step towards the solution of $N_h^2(q_h) = r_h^2$. If a discontinuity in the solution is present, the differences between the results after the first and the second half-step may be considerable. In our case these differences resulted in such large differences in values for q_{ij}^k and q_{ijk}^k, that the numerical flux $f^k(q_{ij}^k, q_{ijk}^k)$ could not properly be evaluated. (The solution of the Riemann problem with the two states q_{ij}^k and q_{ijk}^k shows cavitation.) The responsibility for this problem lies in part on the type of relaxation used: for the non-elliptic Euler equations CSGS-relaxation is not a pure local smoothing procedure. However, we did not succeed in finding a local smoothing procedure that was satisfactory for the Euler equations. E.g. experimentation with a damped collective Jacobi relaxation was not successful.

The Full Multi Grid algorithm

We aim at the approximate solution q_h of the Euler equations for a given mesh and we assume that also L coarser meshes exist. We denote the level of refinement by m and the approximate solution at level m by $q_{(m)} = q_{2^{(L-m)}h}$. The coarser grids, $m < L$, are not only used for the realization of FAS-iteration steps as described in [9,10], but also for the construction of the initial estimate for the iteration process. The algorithm used to obtain the initial estimate and further iterands in the defect correction process is as follows:

(0) start with an approximation for $q_{(0)}$;
(1) **for** $m := 0\ (1)\ L-1$ **do**
(.) **begin**
(1.a) **for** i $:= 1\ (1)\ k_m$ **do** FAS $(N_{(m)}^1\, q_{(m)} = 0)$;
(1.b) $q_{(m+1)} := P_{m+1,m}^1\, q_{(m)}$;
(.) **end;**
(.) $m := L$;
(2) **for** i $:= 1\ (1)\ k_L$ **do** FAS $(N_{(m)}^1\, q_{(m)} = 0)$;
(3) $q_{(m)} := q_{(m)} + P_{m,m-1}^S\, (R_{m-1,m}^0\, q_{(m)} - q_{(m-1)})$;
(4) **for** d $:= 1\ (1)$ deps **do**
(.) **begin**
(4.a) $r_{(m)} := N_{(m)}^1(q_{(m)}) - N_{(m)}^2(q_{(m)})$;
(4.b) **for** i $:= 1\ (1)$ kd **do** FAS $(N_{(m)}^1\, q_{(m)} = r_{(m)})$;
(.) **end;**

Step (1) is an FMG process to obtain a 1st order accurate initial estimate at level L. The prolongation $P_{m+1,m}^1$ is a linear interpolation procedure and, hence, accurate enough to retain the 1st order accuracy on the finer mesh. Asymptotically, the discretization error for $q_{(m)}$ is bounded by $C\, h_{(m)} = \mathcal{O}(2^{L-m}h)$ for $h_{(L)} = h \to 0$. Now a simple analysis shows that, for a fixed $k_m = k$ at all levels, the iteration error at level m is $\approx C h_{(m)}\, s^k / (1 - 2s^k)$, where s is an upper bound for the FAS-convergence factor. Therefore, to obtain a 1st order accurate solution, for iteration (1.a) it is not necessary to reduce the iteration error in $q_{(m)}$ by a factor much smaller than $s^k \approx 1/3$. This means that a single FAS step as described in [9,10] may be sufficient. Not being sure about the validity of the asymptotic assumption, we set $k_m = 2$, $m = 1,2,\ldots,L$. Step (2) is the FAS-iteration to obtain the solution to $N_h^1(q_h) = 0$ up to truncation error accuracy.

Step (3) is a Richardson extrapolation step to find a 2nd order initial estimate for q_h. The prolongation $P_{m,m-1}^S$ and the restriction $R_{m-1,m}^0$ are piecewise bilinear interpolation over superboxes and averaging over cells, respectively, so that $R_{m-1,m}^0 P_{m,m-1}^S = I_{m-1}$ is the identity, and $P_{m,m-1}^S R_{m-1,m}^0$ is a projection operator. With the asymptotic expansion for the error in q_h as

$$q_h = R_h \hat{q} + h^p R_h\, e + \mathcal{O}(h^{p+1}), \tag{4.3}$$

where $\hat{q}$ is the exact solution, we obtain for p = 1 the 2nd order extrapolation

$$R_{2h}\, \hat{q} = 2\, R_{2h,h} q_h - q_{2h} + \mathcal{O}(h^2). \tag{4.4}$$

We find the extrapolated value of q_h in (3) as the sum of (4.4) and $(I_m - P^S_{m,m-1}R^0_{m-1,m})q_h \in \mathrm{Ker}(R_{2h})$. We notice that formally the approximation of $q_{(L)}$ after stage (3) is still $\mathcal{O}(h)$, unless $q_{(L-1)}$ is an $\mathcal{O}(h^2)$ approximation, and stage (2) can reduce the (smooth) error component $R_h e$ by a factor $\mathcal{O}(h)$. Nevertheless, we see in practice that already for small values of k_m, $m = 1,2,...,L$, the Richardson extrapolation can reduce the error significantly.
Step (4) is the defect correction iteration (4.2b). If the defect correction iteration starts with a 1st order initial approximation, for 2nd order accuracy it is sufficient to take dcps=1. This necessitates an improvement of the error by a factor $\mathcal{O}(h)$ in the iteration (4.b), i.e. we need kd = $\mathcal{O}(\log(h))$. However, since the FAS iteration step is the expensive part of the computation in (4), for most purposes we take kd=1 and a sufficiently large number for dcps.

5. NUMERICAL RESULTS

To see the effect of the various different 2nd order schemes and their combination with (a few steps) in the defect correction iteration (4.2), we consider three model problems. We take (1) a smooth subsonic flow through a channel with a curved wall, (2) an oblique shock, and (3) an oblique contact discontinuity. The three problems are all defined on a rectangular domain. The first problem may clearly show the 2nd order accuracy. The other two problems contain the two kinds of discontinuities that may appear in Eulerian flow. In the shock, the characteristics converge and there is a natural mechanism to steepen a smeared shock [5]. In the contact discontinuity the characteristics are parallel and no such mechanism exists. This kind of discontinuity is more like discontinuities that may appear in the solution of the linear convection diffusion equation [8].

We first give a precise description of the 3 problems and then comment on the various numerical results obtained.

Problem 1 The smooth problem.

The domain Ω^* is (-1,1)×(0,1); the coarsest mesh (m=0) contains 4×2 square cells. $y = -1$ is the inflow boundary, with boundary conditions $\rho = 1.0$, $u = 0.75$, $v = 0.0$; $y = 1$ is the outflow boundary: $p = 1/\gamma$; $x = 0$ and $x = 1$ are solid walls: at $x = 1$ we take $v = 0$, and at $x = 0$ we use a slender body approximation for a curved boundary: $v/u = 0.02 \cdot \sin(\pi x)$.
The initial approximation is uniform flow in Ω^* with $\rho = 1.0$, $u = 0.75$, $v = 0.0$ and $p = 1.0$.

Problem 2 The oblique shock

The domain Ω^* is (0,4)×(0,1); the coarsest mesh contains 6×2 cells. The exact solution has 3 subregions with uniform states as given in figure 5.1.

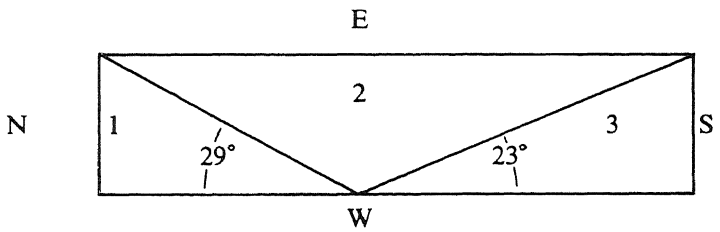

Figure 5.1

The states are resp.:
state 1 : $u = 2.9, v = 0.0, c = 1.0, p = 1.0$;
state 2 : $u = 2.6, v = -0.5, c = 1.1, p = 2.1$;
state 3 : $u = 2.4, v = 0.0, c = 1.2, p = 4.0$.
The boundary conditions are: at N supersonic inflow, at W a solid wall, and at E and S the boundary conditions are overspecified (i.e. for all variables Dirichlet boundary conditions are given, but

these are partly neglected by the difference scheme).

Problem 3 The contact discontinuity

Here $\Omega^* = (0,1)\times(0,1)$, the coarsest mesh is 2×2 cells. The exact solution of the problem has a discontinuity at $x+y = 1$. In both parts of the domain the solution has a uniform state: for $x+y<1$ we take $p = 1.0$, $u = 0.3$, $v = -0.3$ and $c = 0.6$; for $x+y>1$ we have $p = 1.0$, $u = 0.6$, $v = -0.6$ and $c = 1.0$. At the outflow boundaries $p = 1.0$ is given and at the inflow boundaries we give the correct values for u, v and the entropy. The initial estimate has a uniform state over all Ω^* which has mean values between the two uniform states that define the exact solution.

In the figures 5.2 we show for problem 1 the pressure at the curved wall $y = 0$. The results are obtained by the algorithm (0)-(4) described in section 4. In figure 5.2.a the 1st order solution (i.e. the solution after stage (2)) is given for $L = 3,4,5$ and in figure 5.2.b-c we show the second order solutions (at stage (4)) obtained from scheme (3.4) with $\kappa = -1$, after $d = 0$ and $d = 1$ defect correction steps ($k_m = k_L = 4$, kd = 1). I.e. fig. 5.2.b shows the solution before and fig. 5.2.c the solution after the first defect correction step. More defect correction steps ($d>1$), or the use of $\kappa = 1/3$ or the "superbox" scheme all yield very similar pressure profiles.

In figure 5.2.a we see clearly 1st order convergence for the 1st order scheme; 5.2.b and 5.2.c show more accurate solutions. Under assumption of the asymptotic expansion

$$q_h(x,y) = \hat{q}(x,y) + h^p e(x,y) + \mathcal{O}(h^{p+1}),$$

the order of convergence p is derived from the solutions for $L = 3,4,5$, computed as described above. The same computations were made for $\kappa = -1$, $\kappa = 1/3$ and for the "superbox" scheme, both with and without the Richardson extrapolation (i.e. stage (3) of the FMG algorithm). The results are shown in Table 5.1. They seem to confirm the hypothesis of the validity of the asymptotic expansion (4.3) with $p = 1$.

	with Richardson extrapolation			without Richardson extrapolation		
	$\kappa = -1$	$\kappa = 1/3$	SB	$\kappa = -1$	$\kappa = 1/3$	SB
d = 0	2.08	2.08	2.08	1.00	1.00	1.00
d = 1	2.20	1.88	2.23	1.64	1.78	1.50
d = 2	2.11	1.93	1.81	2.18	1.83	1.50
d = 3	1.88	2.01	1.96	1.88	2.13	2.02
d = 4	2.15	1.93	1.96	2.10	1.99	1.95
d = 5	1.92	1.92	1.92	1.98	1.93	1.92

Table 5.1. The measured (mean) order of convergence (at cell corners, boundaries excluded). The second order schemes are (3.4) with $\kappa = -1$ and $\kappa = 1/3$, and (SB) the "superbox" scheme.

For problem 2 we show results in the figures 5.3. For the level $L = 4$ we show the 1st order solution, the solution obtained after Richardson extrapolation and the solution after 1 and 3 defect correction steps.

In the figures 5.4 we show the same results for problem 3. For the problems 2 and 3 results are shown only for the scheme (3.4) with $\kappa = -1$. From the figures 5.3 and 5.4 it is clear that not only a higher order of accuracy is obtained; we also find a better resolution of skew discontinuities.

ACKNOWLEDGEMENT

I want to acknowledge the cooperation with B. Koren, S. Spekreijse and P.M. de Zeeuw in this Euler research. The investigations were supported in part by the Netherlands Technology Foundation (STW).

REFERENCES

[1] Anderson, W.K., Thomas, J.L., and Van Leer, B., "A comparison of finite volume flux vector splittings for the Euler equations" AIAA Paper No. 85-0122.
[2] Böhmer, K., Hemker, P. & Stetter, H., "The Defect Correction Approach." Computing Suppl. 5 (1984) 1-32.
[3] Brandt, A., "Guide to Multigrid Development." In: Multigrid Methods (W. Hackbusch and U. Trottenberg eds), Lecture Notes in Mathematics 960, pp.220-312, Springer Verlag 1982.
[4] Colella, P. and Woodward, P.R., "The Piecewise Parabolic Method (PPM) for Gas Dynamical Simulations" J. Comp. Phys 52 (1984) 174-201.
[5] Davis, S.F., "A rotationally biased upwind difference scheme for the Euler equations." J. Comp. Phys. 57 (1984) 65-92.
[6] Hackbusch, W., "Bemerkungen zur iterierten Defektkorrektur und zu ihrer Kombination mit Mehrgitterverfahren." Rev. Roum. Math. Pures Appl. 26 (1981) 1319-1329.
[7] Harten, A., Lax, P.D. & Van Leer, B., "On upstream differencing and Godunov-type schemes for hyperbolic conservation laws." SIAM Review 25 (1983) 35-61.
[8] Hemker, P.W., "Mixed defect correction iteration for the solution of a singular perturbation problem." Comp. Suppl. 5 (1984) 123-145.
[9] Hemker, P.W. & Spekreijse, S.P., "Multigrid solution of the Steady Euler Equations." In: Advances in Multi-Grid Methods (D.Braess, W.Hackbusch and U.Trottenberg eds) Proceedings Oberwolfach Meeting, Dec. 1984, Notes on Numerical Fluid Dynamics, Vol.11, Vieweg, Braunschweig, 1985.
[10] Hemker, P.W. & Spekreijse, S.P., "Multiple Grid and Osher's Scheme for the Efficient Solution of the the Steady Euler Equations." (Report NM-8507, CWI, Amsterdam, 1985.) To appear in Applied Numerical Mathematics.
[11] Jameson, A., "Numerical Solution of the Euler Equations for Compressible Inviscid Fluids." In: Procs 6th International Conference on Computational Methods in Applied Science and Engineering, Versailles, France, Dec. 1983.
[12] Jespersen, D.C. "Design and implementation of a multigrid code for the steady Euler equations." Appl. Math. and Computat. 13 (1983) 357-374.
[13] Jespersen, D.C. "Recent developments in multigrid methods for the steady Euler equations." Lecture Notes, March 12-16, 1984, von Karman Inst., Rhode-St.Genese, Belgium.
[14] G.M. Johnson, "Multiple grid convergence acceleration of viscous and inviscid flow computations." Appl. Math. and Computat. 13 (1983) 375-398.
[15] Lax, P.D., "Hyperbolic systems of conservation laws and the mathematical theory of shock waves." Regional conference series in applied mathematics 11. SIAM Publication, 1973
[16] Lax, P.D., "Shock waves and entropy" In: Contributions to Nonlinear Functional Analysis (E.H. Zarantonello ed.) Acad. Press, New York, 1971.
[17] Mulder, W.A. "Multigrid Relaxation for the Euler equations." To appear in: J. Comp. Phys. 1985.
[18] Ni Ron-Ho , "A multiple grid scheme for solving the Euler equations." AIAA Journal 20 (1982) 1565-1571.

[19] Osher, S. "Numerical solution of singular perturbation problems and hyperbolic systems of conservation laws", In: Analytical and Numerical Approaches to Asymptotic problems in Analysis, O. Axelsson, L.S. Frank and A. van der Sluis eds.), North Holland Publ. Comp., 1981.
[20] Osher, S. & Chakravarthy, S., "High resolution schemes and the entropy condition." SIAM J. Numer. Anal. 21 (1984) 955-984.
[21] Osher, S & Solomon, F., "Upwind difference schemes for hyperbolic systems of conservation laws." Math. Comp. 38 (1982) 339-374.
[22] Schmidt, W. and Jameson, A., "Euler solvers as an analysis tool for aircraft aerodynamics." In: Advances in Computational Transonics (W.G.Habashi (ed.) Pineridge Press, Swansea.
[23] Spekreijse, S. "Second order accurate upwind solutions of the 2D steady state Euler equations by the use of a defect correction method." CWI-report, in preparation, 1985.
[24] Steger, J.L., "A preliminary study of relaxation methods for the inviscid conservative gasdynamics equations using flux splitting." Nasa Contractor Report 3415 (1981).
[25] Steger, J.L. & Warming, R.F., "Flux vector splitting of the inviscid gasdynamics equations with applications to finite difference methods." J. Comp. Phys. 40 (1981) 263-293.
[26] Sweby, P.K. "High resolution schemes using flux limiters for hyperbolic conservation laws", SIAM J.Numer.Anal. 21 (1984) 995-1011.
[27] Van Leer, B., "Flux-vector splitting for the Euler equations." In: Procs. 8th Intern. Conf. on numerical methods in fluid dynamics, Aachen, June, 1982. Lecture Notes in Physics 170, Springer Verlag.
[28] Van Leer, B., "Upwind difference methods for aerodynamic problems governed by the Euler equations" Report 84-23, Dept. Math. & Inf., Delft Univ. Techn., 1984.
[29] Van Leer, B. and Mulder, W.A., "Relaxation methods for hyperbolic conservation laws." In: Dynamics of Gas in a rotating Galaxy (W.A. Mulder, thesis, Leiden Univ., 1985).
[30] de Zeeuw, P.M. and van Asselt, E.J., "The convergence rate of multi-level algorithms applied to the convection diffusion equation." SIAM J.S.S.C. 6 (1985) 492-503.

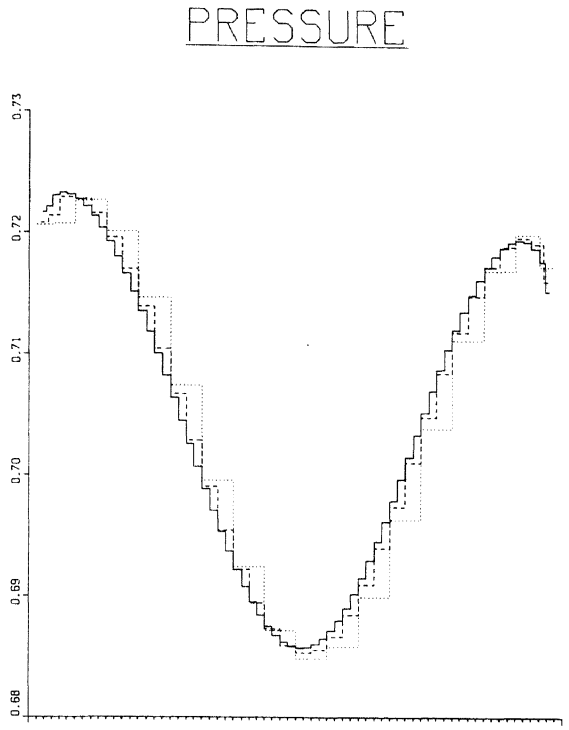

Figure 5.2.a Problem 1. The 1st order solution.

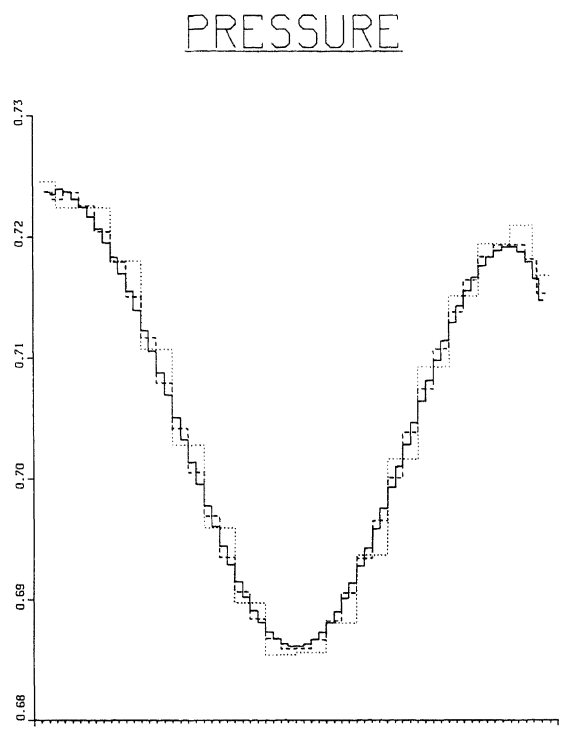

Figure 5.2.b Problem 1.
The 2nd order solution [(3.4) with $\kappa = -1$], dcps = 0.

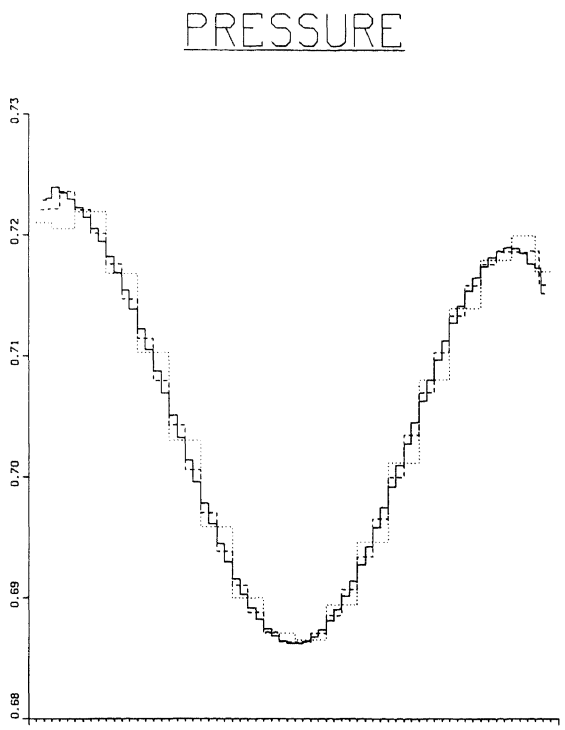

Figure 5.2.c Problem 1. The 2nd order solution [(3.4) with $\kappa = -1$], dcps = 1.

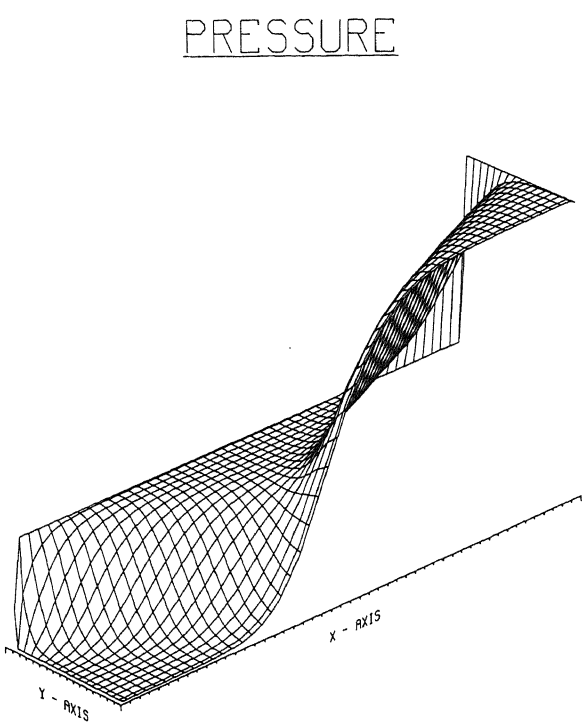

Figure 5.3.a Problem 2. The 1st order solution.

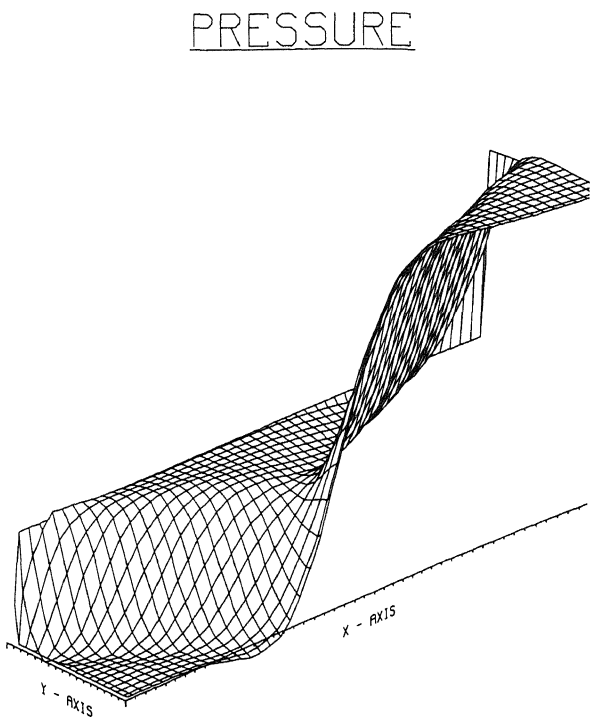

Figure 5.3.b Problem 2.
The 2nd order solution after Richardson extrapolatio

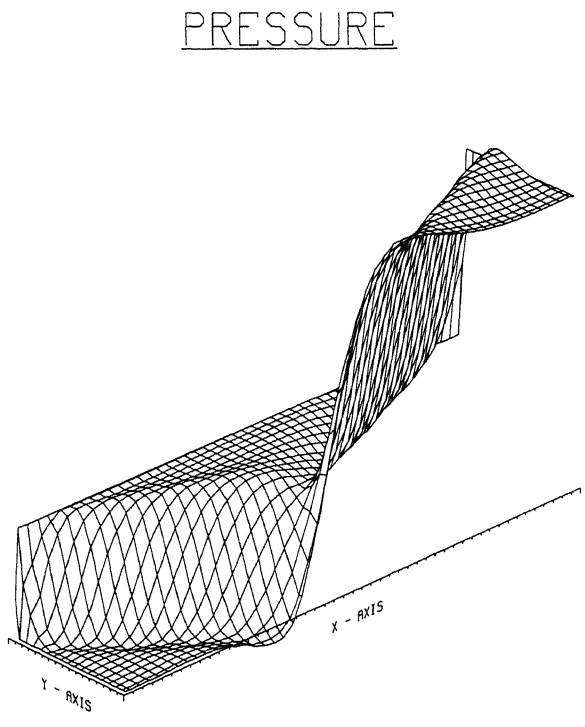

Figure 5.3.c Problem 2. After 1 DCP step

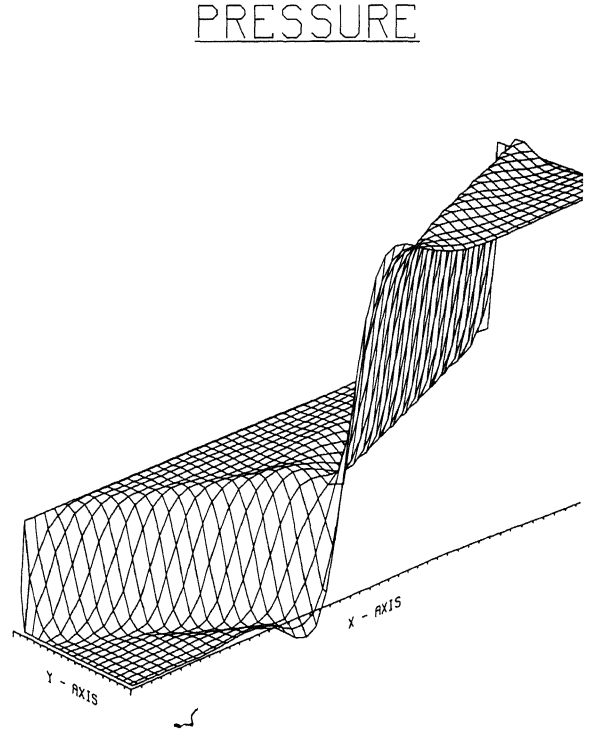

Figure 5.3.d Problem 2. After 3 DCP steps

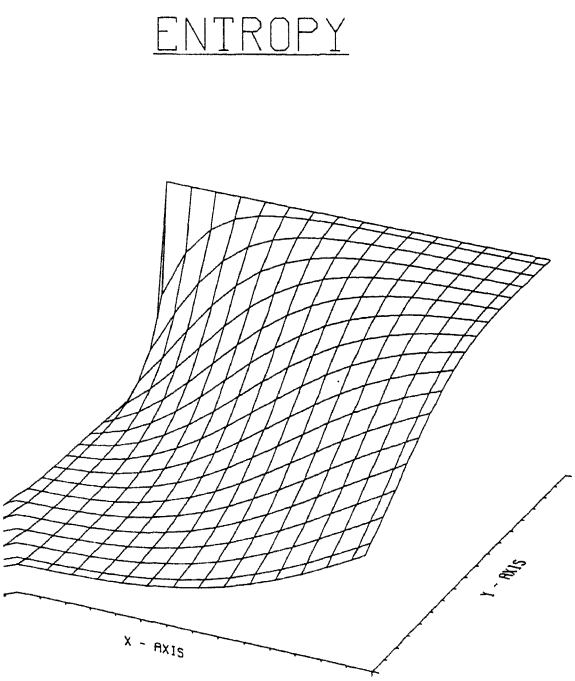

5.4.a Problem 3. The 1st order solution.

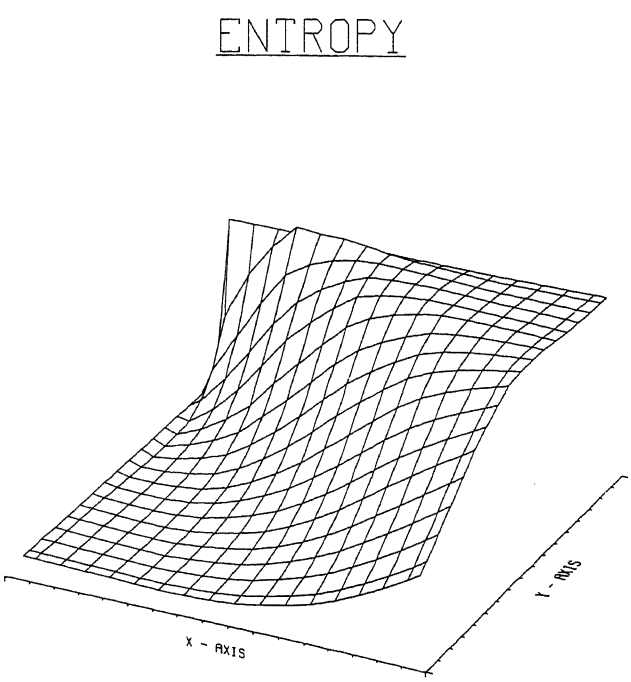

Figure 5.4.b Problem 3.
The 2nd order solution after Richardson extrapolation.

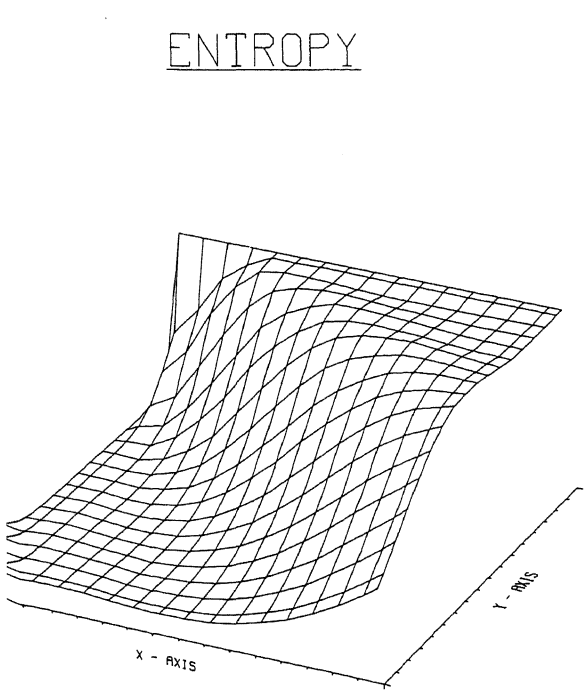

ure 5.4.c Problem 3. After 1 DCP step

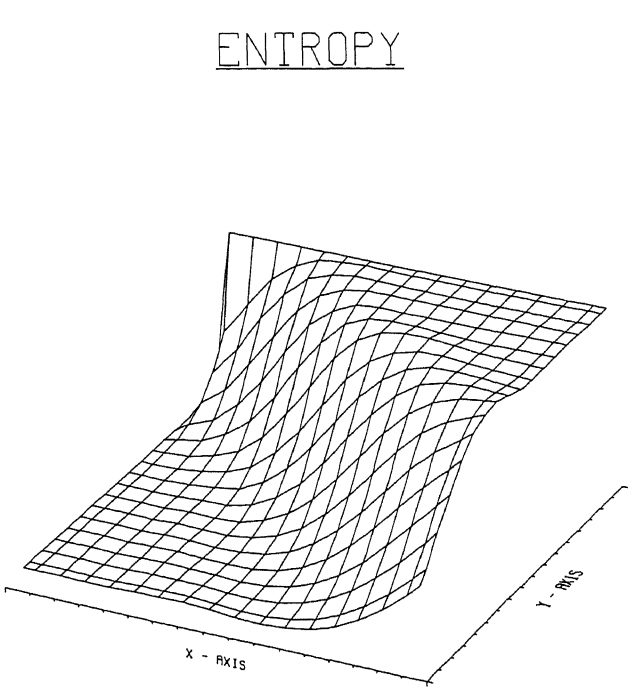

Figure 5.4.d Problem 3. After 3 DCP steps